ISSN 1726-5749

SENSORS & TRANSDUCERS

vol. 90 Special 4/08

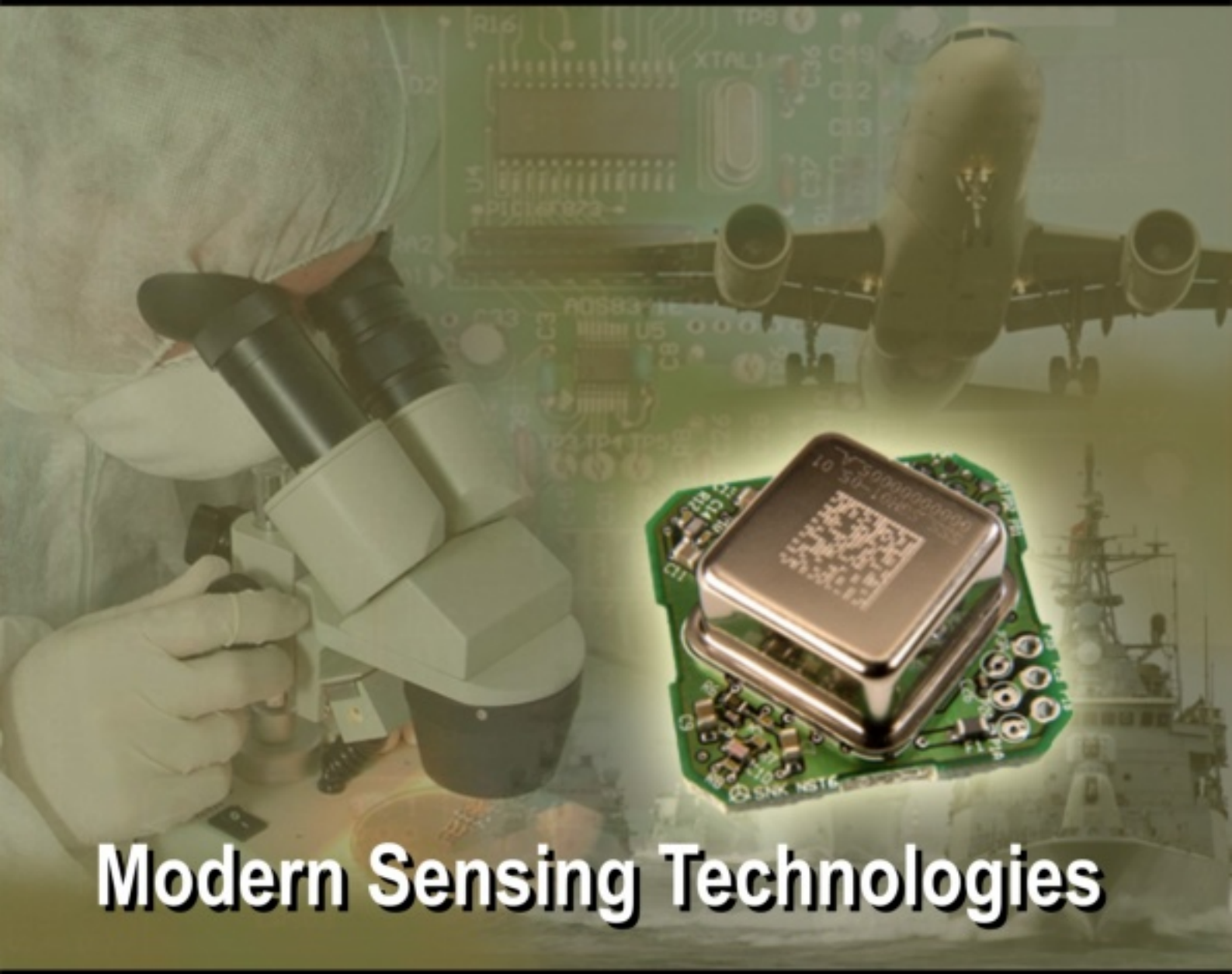

Modern Sensing Technologies

International Frequency Sensor Association Publishing

IFSA

Sensors & Transducers

Special Issue
April 2008

www.sensorsportal.com

ISSN 1726-5479

Sensors & Transducers Journal (ISSN 1726-5479) is a peer review international journal published monthly online by International Frequency Sensor Association (IFSA). Available in electronic and CD-ROM.

Sensors & Transducers Journal

Contents

Volume 90
Special Issue
April 2008

www.sensorsportal.com

ISSN 1726-5479

Special Issue on Modern Sensing Technologies

Editorial

Sensors for Medical/Biological Applications

Wireless Sensors

Capacitive Sensors

Sensors Signal Processing

Gas Sensors

Image Sensors

Miscellaneous

Authors are encouraged to submit article in MS Word (doc) and Acrobat (pdf) formats by e-mail: editor@sensorsportal.com
Please visit journal's webpage with preparation instructions: http://www.sensorsportal.com/HTML/DIGEST/Submition.htm

Sensors & Transducers Journal, Vol. 90, Special Issue, April 2008, pp. 195-208

www.sensorsportal.com

Sensors & Transducers

ISSN 1726-5479

http://www.sensorsportal.com

Calibration-free Image Sensor Modelling Using Mechanistic Deconvolution

Shen Hin Lim, Tomonari Furukawa
University of New South Wales, Sydney, Australia
E-mail: shen.lim@student.unsw.edu.au

Received: 15 October 2007 /Accepted: 20 February 2008 /Published: 15 April 2008

Abstract: This paper presents a calibration-free approach to modelling image sensors using mechanistic deconvolution, whereby the model is derived using mechanical and electrical properties of the sensor. In this approach, effective focal length is determined using thick lens properties approximated from lens system. The accumulated uncertainties and constraints from sensor properties are utilized with approximated aperture stop position offset to estimate distortion effects, and, eventually to derive corrected image data. This reduces dependency on image data, and, as a result, does not require experimental setup or calibration. An experiment was constructed to evaluate accuracy of model created by the approach, and its robustness to changes in sensor properties without recalibration. The model was compared with a pre-calibrated model using two sensors with different specifications. The model achieved similar accuracy with one-fifth of number of iterations. The approach was also shown to be robust and, in comparison to pre-calibrated model, improved the accuracy significantly. *Copyright © 2008 IFSA.*

Keywords: Image sensor, Sensor modelling, Mechanistic deconvolution, Lens distortion, Calibration

1. Introduction

As off-the-shelf image sensors are not perfect, information obtained from them cannot be perfectly accurate. Consequently, corrective sensor modelling, also known as calibration, is an important process for applications that require accurate geometric measurements [1]. In addition, the process needs to be computationally inexpensive for real-time applications. The process has long been an important issue in photogrammetry and computer vision fields, and more recently, in the area of robotics and automation, for example, mobile robot navigation [2].

Conventionally, sensors have been corrected by either iteratively applying non-linear optimization, or analytically deriving a closed-form solution. The former technique utilizes the initial guess of sensor parameters, to derive a non-linear solution iteratively and attains accurate calibration [3, 4]. This technique, however, requires good estimation of the initial guess for accurate calibration and is computationally expensive. On the contrary, the computationally inexpensive closed-form solution is derived by a set of linear equations, which do not take distortion into account and yield inaccurate results [3, 5]. The disadvantages in these classical techniques have motivated the researchers to develop new techniques, which may be categorized into two groups: the two-step method [3, 5-9], and self-calibration [10-12].

The two-step method was proposed by Tsai [3]. A closed-form solution is initially derived using radial alignment constraints to estimate extrinsic parameters and effective focal length. The parameters are then used to derive a non-linear solution iteratively and retrieve radial distortion parameter and corrected effective focal length. This technique reduces the number of required iterations considerably. Weng et al. [5] improved the two-step method and successfully estimated tangential distortion parameters. A number of other groups have also proposed techniques that derive radial distortion parameters analytically, prior to finding a non-linear solution iteratively, in an attempt to reduce the number of iterations [6, 7]. Similarly, Bailey [8] derived an analytical solution to estimate the parameters using parabolic curves. For real-time applications, Park and Hong [9] simplified Tsai's technique by applying look-up-table (LUT) techniques.

Maybank et al. [10] developed a different type of calibration technique, namely self-calibration. In contrast to the two-step method, this technique does not require a calibration setup that includes a calibration object with known 3D geometrical features. The intrinsic parameters are assumed to be constant to reduce computational expenses. In comparison to other technique, this method requires at least three different orientations and achieves lower accuracy, despite having higher flexibility. The self-calibration technique has been modified and extended to include different constraints, mainly camera motion and scene constraints, to increase its accuracy [11]. Zhang [12] has fused this technique with the two-step method and was able to reduce number of orientations whilst having better robustness, as compared to the self-calibration.

These techniques have a common approach; the image sensor is evaluated with a known image. These models have shown to reproduce parameters of image sensor successfully, negating the need to manually obtain the sensor's mechanical and electrical properties. Nevertheless, the sensor model derived from these properties may also derive image sensor parameters and reduce the dependency of the image quality, and, acts as an alternative solution to calibration.

This paper presents a calibration-free approach to modelling image sensors using mechanistic deconvolution. The proposed approach evaluates the image sensor using its mechanical and electrical properties. A thick lens, which determines the effective focal length, is used to approximate the sensor lens system. In contrast to conventional models, distortion model is developed using uncertainties and constraints present in the sensor. The approach also uses aperture stop position offset to further evaluate lens distortion effect. In this approach, three assumptions are made: firstly, a distance between sensor and its plane of view is known; secondly, image plane is orthogonal to its z-axis; thirdly, only radial distortion is considered. One advantage of this approach is the removing requirement of experimental evaluation of image sensors, while remaining robust to changes in its properties.

The paper is organized as follows. Section 2 reviews the general formulation of existing problem and techniques. The model derived from the proposed approach, namely mechanistic deconvolutive model is presented in Section 3. This is followed by numerical examples in Section 4, including experimental setup and procedure. Finally, Section 5 presents the conclusion of this paper.

2. Conventional Sensor Models

2.1. Pinhole Camera Model

The transformation from object world coordinate system to image plane is shown in this sub-section, and, its formulations are based on pinhole camera model; that is the ideal form of image sensor model. Initially, the position of an object with respect to the world coordinate system, $\mathbf{x}_w=[x_w, y_w, z_w]^T$, is transformed to that with respect to the camera 3D coordinate system, $\mathbf{x}_p=[x_p, y_p, z_p]^T$, as

$$\mathbf{x}_p = \mathbf{R}\mathbf{x}_w + \mathbf{t}, \tag{1}$$

where **R** is the rotational matrix and **t** is the translational vector. The **R** and **t** are known as the extrinsic parameters. The position $\mathbf{x}_p$ is then converted to the image plane coordinate system, $\mathbf{x}_u=[u, v, 1]^T$, using its z-component and intrinsic parameters in **A**:

$$\mathbf{x}_u = \mathbf{A}\mathbf{x}_p \tag{2}$$

Here A, formulated on the assumption that the image plane axes are parallel to the world coordinate system, is given by

$$\mathbf{A} = \begin{bmatrix} f_x & 0 & u_0 \\ 0 & f_y & v_0 \\ 0 & 0 & 1 \end{bmatrix} \quad \text{with} \quad \left\{ \begin{array}{l} f_x = f \big/ p_x \\ f_y = f \big/ p_y \end{array} \right\}, \tag{3}$$

where f is the effective focal length, $[u_0, v_0]$ is the principal point coordinates and $\mathbf{p}_s=[p_x, p_y]^T$ is the pixel size.

2.2. Distortion Model

The previous sub-section considers the ideal form of sensor model, and unable to include the distortion effects inherent in image sensors. These effects, namely radial and tangential distortions, produce the distorted coordinates, $\mathbf{x}_d=[u_d, v_d]^T$. Hence, by using $\mathbf{x}_d$, the corrected image data coordinates, also known as undistorted coordinates $\mathbf{x}_u$ are

$$\mathbf{x}_u = \left(1 + \sum_1 K_i \left(r_d^{2i} - 1\right)\right)\mathbf{x}_d + \mathbf{g}, \tag{4}$$

where $K_{1:i}$ are radial distortion factors, and **g** and r_d are as follows

$$\mathbf{g} = \begin{bmatrix} P_1\left(r_d^2 + 2u_d^2\right) + 2P_2 u_d v_d \\ P_2\left(r_d^2 + 2v_d^2\right) + 2P_1 u_d v_d \end{bmatrix} \tag{5}$$

$$r_d = \sqrt{u_d^2 + v_d^2}, \tag{6}$$

where P_1 and P_2 are tangential distortion factors. It is noted that image data are highly affected by radial distortion.

2.3. Conventional Model Approach

The previous sub-sections have shown that quality of image data is a dominant factor for modelling a given sensor. Fig. 1 illustrates the general approach of conventional models. The image data ${}^{s}I$ is initially utilized to estimate initial extrinsic and intrinsic parameters **A**, **R** and **t**, by deriving a closed-form solution using (1)–(3). The initial parameters are then used with other inputs, which are target geometric features and radial alignment constraint, to determine initial distortion factors K_1 and K_2 as defined in (4). The derived **A**, **R**, **t**, K_1 and K_2 are inserted into the non-linear optimization process with given ${}^{s}I$ such that these parameters satisfy (1)–(6). The parameters obtained from non-linear optimization process derive undistorted coordinates $\mathbf{x}_u$, and, obtain the corrected image eventually.

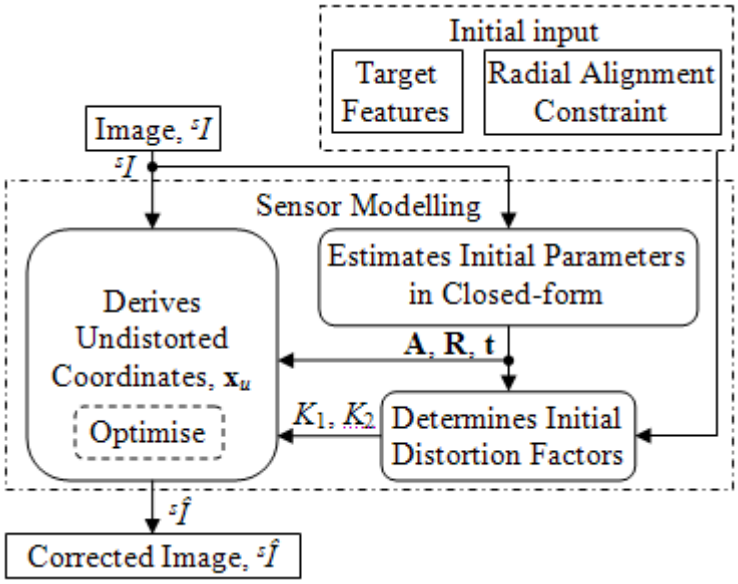

Fig. 1. Conventional technique.

3. Mechanistic Deconvolutive Model

3.1. Determining Effective Focal Length Using Optical Parameters

In contrast to the conventional models, the proposed approach determines the effective focal length of the sensor by its lens system. Initially, the complex lens system is approximated by a thick lens system, to reduce required parameters and complexity. The thick lens system is defined as follows [13],

$$\frac{1}{f} = (n-1)\left[\frac{1}{r_1} - \frac{1}{r_2} + \frac{t(n-1)}{nr_1r_2}\right], \tag{7}$$

where n is the refractive index, r_1 and r_2 are the radii of curvature closest and farthest from the light source, and t is the overall lens thickness. By rearranging equation (7), the effective focal length f becomes

$$f = \frac{nr_1r_2}{(n-1)\left(nr_2 - n_1r_1 + t(n-1)\right)} \tag{8}$$

This equation shows that three components provide uncertainties in f; r_1, r_2 and t, which can be well approximated as Gaussian noise. This produces the modified effective focal length f_d, as follows

$$f_d = f + w^f , \tag{9}$$

where w^f is the combination of uncertainties from r_1, r_2 and t.

3.2. Deriving Undistorted Coordinates Using Constraints, Uncertainties and Aperture Stop Position

3.2.1. Constraints and Uncertainties

A general image sensor is constrained by three elements that are the pixel size, sensor chip, and diameter aperture. The pixel size, $\mathbf{p}_s$ controls the possible smallest size of scene feature. This is defined as the feature resolution constraint, with its parameter $(\mathbf{b}_1-\mathbf{b}_2)_{\min}$. It is also constrained by f_d and the distance between the scene feature and sensor, l as

$$\left(\mathbf{b}_1 - \mathbf{b}_2\right)_{\min} - \frac{l}{f_d}\mathbf{p}_s \geq 0 , \tag{10}$$

where $\mathbf{b}_1=[x_{b1}, y_{b1}]^{\mathrm{T}}$ and $\mathbf{b}_2=[x_{b2}, y_{b2}]^{\mathrm{T}}$ are the reference points that define the size vector of scene feature. The sensor chip acts as a field stop, and hence its size, $\mathbf{s}_a=[s_x, s_y]^{\mathrm{T}}$ controls the size of the largest scene feature. Using $\mathbf{p}_s$ and the pixel resolution $\mathbf{p}_r=[p_r^x, p_r^y]^{\mathrm{T}}$, $\mathbf{s}_a$ is

$$\mathbf{s}_a = \mathbf{p}_r \cdot \mathbf{p}_s \tag{11}$$

The field of view constraint is derived in the following manner,

$$\frac{2ls_i \tan\left(\theta_d/2\right)}{s_d} - \left|\left(\mathbf{b}_1 - \mathbf{b}_2\right)\cdot \mathbf{e}_i\right|_{\max} \geq 0; i = x : y , \tag{12}$$

where $(\mathbf{b}_1-\mathbf{b}_2)_{\max}$ is the field of view constraint parameter, θ_d is the field of view angle, and $s_d=(s_x^2+s_y^2)^{0.5}$. The angle θ_d can also be derived as follows,

$$\theta_d = 2\tan^{-1}\left(s_d/2f_d\right) \tag{13}$$

Equation (13) is rearranged and becomes

$$\tan\left(\theta_d/2\right) = \frac{s_d}{2f_d} \tag{14}$$

and is substituted into equation (12), to obtain

$$\frac{l}{f_d}\mathbf{s}_a - \left(\mathbf{b}_1 - \mathbf{b}_2\right)_{\max} \geq 0 \tag{15}$$

and shows that f_d and $\mathbf{s}_a$ are the factors that affect the field of view constraint. Lastly, the final

constraint, also known as the depth of field constraint, is affected by the diameter aperture size. In normal cases, the diameter aperture size d_a is used as the aperture stop to limit the *number of rays*, and resultantly affects the image brightness, I_b. The relationship between I_b, d_a and f_d is

$$I_b \propto \left({}^{d_a}\!/\!_{f_d} \right)^2 \tag{16}$$

The aperture stop also changes the exposure time t_e, as follows

$$t_e \propto {}^{1}\!/\!_{I_b} = \left({}^{n_f}\!/\!_{\sqrt{2}} \right)^2, \tag{17}$$

where n_f is the f-number, a different representation of t_e. By introducing a linear constant q, (16) and (17) can be combined and n_f is formulated as

$$n_f = \sqrt{\frac{2}{q}} \left(\frac{f_d}{d_a} \right) \tag{18}$$

The image brightness I_b indirectly affects the focus of the sensor, because it is highly dependent on t_e. This brings forth a new term, namely the depth of field D_f and is defined as the range where the image is considered in focus. The depth of field D_f is derived by the following equations,

$$D_f^{-} = \frac{hl}{h+l} \tag{19}$$

$$D_f^{+} = \begin{cases} \dfrac{hl}{h-l}; l < h \\ \infty; l > h \end{cases} \tag{20}$$

$$D_f = D_f^{+} - D_f^{-}, \tag{21}$$

where D_f^+ and D_f^- are the far and near limit of depth of field respectively, and h is the depth of field constraint parameter. The h is actually the hyperfocal distance and is defined as the distance between the sensor and the object plane when the lens system is most focused. The formulation of h is

$$h = \frac{f_d^{\,2}}{n_f c}, \tag{22}$$

where c is the set limit of blurriness. By substituting n_f defined in equation (18), h becomes

$$h = \sqrt{\frac{q}{2}} \left(\frac{f_d d_a}{c} \right) \tag{23}$$

This shows that c plays an important part in determining the hyperfocal distance. In this approach, c is given an approximation of 0.1% of f_d. Hence, h is redefined as follows,

$$h = 1000 d_a \sqrt{\frac{q}{2}} \tag{24}$$

and validates that h is indeed affected by d_a. Similar to other lens properties, d_a also has its own tolerance and represented as Gaussian noise. This produces a new hyperfocal distance h_d,

$$h_d = h + v^h , \tag{25}$$

where v^h is the estimated uncertainties based on d_a. Finally, the constraint parameters are used with f_d and l to develop the undistorted coordinates $\mathbf{x}_u$ function, represented as

$$\mathbf{x}_u = \mathrm{f}_1\left(f_d, \left(\mathbf{b}_1 - \mathbf{b}_2\right)_{\min}, \left(\mathbf{b}_1 - \mathbf{b}_2\right)_{\max}, l, h_d\right) \tag{26}$$

3.2.2. Aperture Stop Position

The derived undistorted coordinates function in equation (26) does not include lens distortion. The proposed approach develops the distortion model using the aperture stop position offset from the principal plane of the approximated lens system, m_a. In this approach, only radial distortion is considered. The approach is initially described based on one axis. Lens distortion, $\boldsymbol{\delta}$ is

$$\boldsymbol{\delta} = \mathbf{y}' - \mathbf{y} , \tag{27}$$

where $\mathbf{y}'=[y_1', y_2', y_3', \ldots]^{\mathrm{T}}$ and $\mathbf{y}=[y_1, y_2, y_3, \ldots]^{\mathrm{T}}$ are the distorted and undistorted image position coordinates. Using the thick lens approximation described in Section 3.1 and the small angle approximation, $\mathbf{y}$ and $\mathbf{y}'$ are

$$\mathbf{y} = f_d \tan \boldsymbol{\theta}_1 \text{ and} \tag{28}$$

$$\mathbf{y}' = m_a \tan \boldsymbol{\theta}_2 , \tag{29}$$

where $\boldsymbol{\theta}_1$ and $\boldsymbol{\theta}_2$ are the refracted angles of the ray based on the position of aperture stop and the principal plane respectively. Both $\mathbf{y}$ and $\mathbf{y}'$ are projected from the same object, and hence, the relationship between $\boldsymbol{\theta}_1$ and $\boldsymbol{\theta}_2$ is

$$l \tan \boldsymbol{\theta}_1 = \left(l - m_a\right) \tan \boldsymbol{\theta}_2 , \tag{30}$$

where l is previously defined as the distance between the scene feature and the sensor. Equation (30) is rearranged as following,

$$\tan \boldsymbol{\theta}_1 = \frac{l - m_a}{l} \tan \boldsymbol{\theta}_2 \tag{31}$$

to obtain more distinct relationship between $\boldsymbol{\theta}_1$ and $\boldsymbol{\theta}_2$, and, using equation (27)-(31), $\boldsymbol{\delta}$ then becomes

$$\boldsymbol{\delta} = \left(m_a \left(1 + \frac{f_d}{l} \right) - f_d \right) \tan \boldsymbol{\theta}_2 \tag{32}$$

Using the pixel resolution $\mathbf{p}_r$, this is then expanded to both axes, and derive the distorted coordinates $\mathbf{x}_d$,

$$\mathbf{x}_d = \mathrm{f}_2\left(f_d, m_a, l, \boldsymbol{\theta}_x, \boldsymbol{\theta}_y, \mathbf{p}_r\right), \tag{33}$$

where $\boldsymbol{\theta}_x$ and $\boldsymbol{\theta}_y$ are the refracted angles based on the position of the aperture stop in x and y direction. The $\mathbf{x}_d$ are then included as a factor of $\mathbf{x}_u$ shown in equation (26), and $\mathbf{x}_u$ are reformulated as

$$\mathbf{x}_u = \mathrm{g}\left(f_d, \left(\mathbf{b}_1 - \mathbf{b}_2\right)_{\min}, \left(\mathbf{b}_1 - \mathbf{b}_2\right)_{\max}, l, h_d, \mathbf{x}_d\right) \tag{34}$$

Fig. 2 shows the mechanistic deconvolution approach. In contrast to the conventional technique illustrated in Fig. 1, the required parameters in modelling a given sensor are determined by its mechanical and electrical properties, instead of image data ${}^{s}I$. The effective focal length, f_d is estimated by the thick lens parameters of the sensor, which are the radii curvatures r_1 and r_2, the refractive index n and the lens thickness t. These parameters are obtained by the thick lens approximation of the actual sensor lens system. The calculated f_d is then used with other mechanical and electrical properties $\mathbf{z}$, and the distance between the scene feature and the sensor l to determine the constraint parameters, $\mathbf{c}_p$ and the distorted coordinates, $\mathbf{x}_d$. The undistorted coordinates, $\mathbf{x}_u$ are derived using previously estimated f_d, $\mathbf{x}_d$ and $\mathbf{c}_p$, and finally, $\mathbf{x}_u$ are used to determine the corrected image data ${}^{s}\hat{I}$.

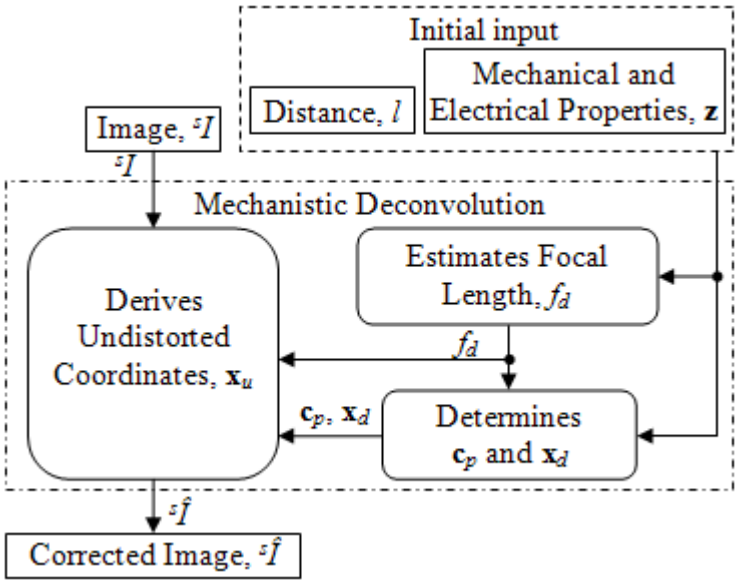

Fig. 2. Proposed technique.

4. Numerical Examples

An experimental setup was constructed to evaluate the mechanistic deconvolution approach in terms of accuracy and robustness to changes in image sensor properties without recalibration. The target used in this experimental setup was grid a pattern of 20 by 18 boxes. Two image sensors with different specifications, as shown in Table 1, were used in the evaluation process. It is noted that Case 1 has better specifications than Case 2. Focus of the sensors is manually adjusted, which acts as the only similarity between image sensors.

Table 1. Specifications of the image sensors.

Specifications	**Case 1**	**Case 2**
Pixel Resolution (Mpixel)	2	0.4
Sensor Type	CCD	CMOS
Sensor Size, $\mathbf{s}_a$ (mm)	11.8X7.9	2.6X2.13
Aperture Stop Position Offset, m_a (mm)	0.1	0.2
Lens thickness, t (mm)	4	3

The approach was compared with a conventional technique discussed in Section 2. The optimization technique used by conventional approach was Gauss-Newton method. Accuracy of both approaches was evaluated by determining radii mean error, when compared with the ideal form of grid pattern. The formulation of radii mean error is given in the Appendix section. Robustness of the approaches was then tested by changing two factors of sensor properties, which are aperture stop position offset from the principal plane, m_a and lens thickness, t.

Fig. 3 shows an example of original images taken by two image sensors specified in Table 1, and, their corrected images using proposed approach, namely mechanistic deconvolution. Note that Figs. 3(a) and 3(c) are the original images while Figs. 3(b) and 3(d) are the corrected images. Using accuracy evaluation mentioned above, the corrected image percentage error of Case 1 and Case 2 are 0.8 % and 2.5 % respectively. It is illustrated that the mechanistic deconvolution approach managed to provide a highly accurate corrected image, despite being affected by the image sensors different specifications.
Fig. 4 illustrates further evaluation of Fig. 3 corrected images accuracy, in comparison to conventional approach, and, the required number of iterations to achieve minimal percentage error for each sensor. Fig. 4(a) is an example of original image taken from Case 2 sensor, Figs. 4(b) and 4(c) are corrected images using proposed and conventional approaches based on Fig. 4(a), and, Fig. 4(d) gives the numerical results of the further evaluation process mentioned previously. Figs. 4(b) and 4(c) show that the accuracy of the corrected image by the proposed approach is similar to the conventional approach corrected image. This evaluation is further supported by the radii mean error illustrated in Fig. 4(d), which is 2.3 %. Fig. 4(d) also provides that the radii mean error for corrected images using the proposed and conventional approaches, based on the example of original image shown in Fig. 3(a), are similar as well, approximately 1 %. The proposed approach, however, reduced required the number of iterations by a factor of 2.5 for Case 1 and 5 for Case 2, in comparison to conventional method, as shown in Fig. 4(d).

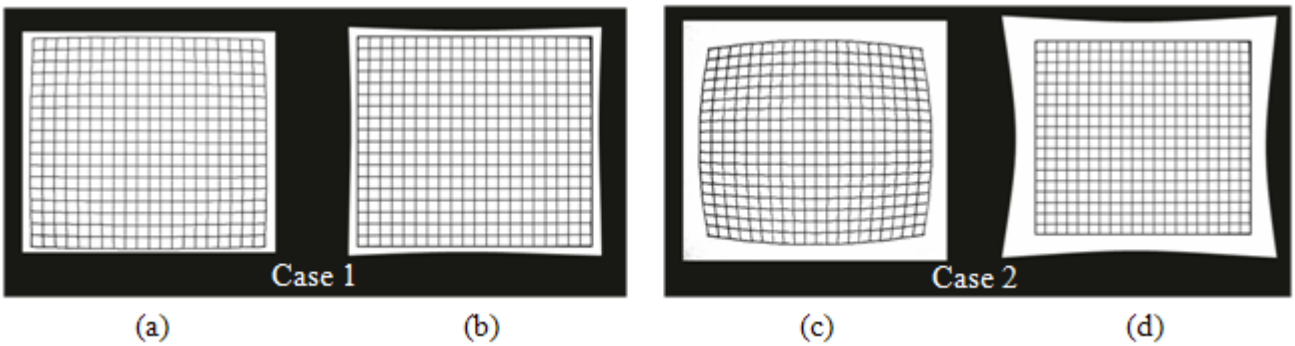

Fig. 3. Original and Corrected Image for Both Cases Using Proposed Approach.

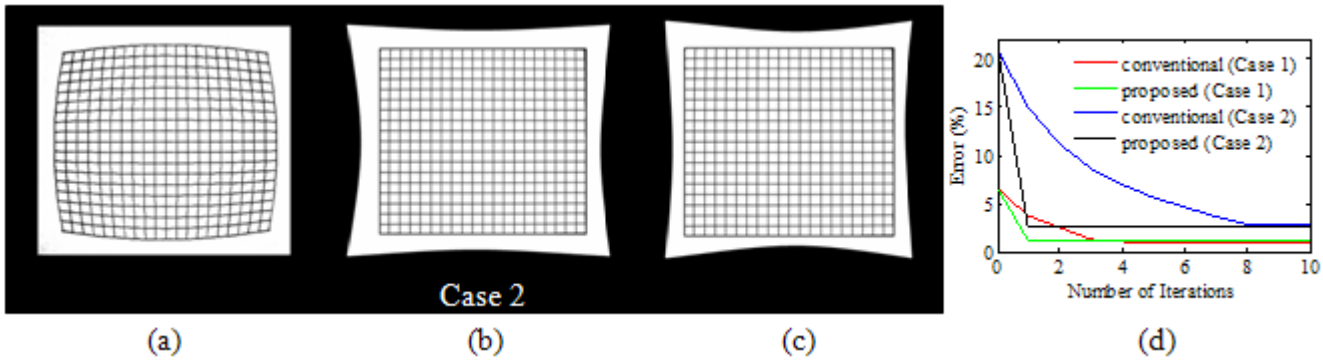

Fig. 4. Corrected Images of Proposed and Conventional Approaches and Accuracy Evaluation in Corresponding to Number of Iterations.

Fig. 5 presents the original images of sensor Case 2, and, corrected images using the proposed and conventional approaches, due to changes in sensor properties that are aperture position offset m_a and lens thickness t. Figs. 5(a) – 5(c) are based on the changes in m_a value from 0.2 to 0.5 while Figs. 5(d) – 5(f) are based on the changes in t value from 3 to 5. The corrected images using the proposed approach, as illustrated in Figs. 5(b) and 5(e), manage to show that the approach are not affected by the changes in m_a and t, and, provide the radii mean error of 1.1 % and 2.6 % respectively. The corrected images using the conventional approach, however, are affected by these changes as shown in Figs. 5(c) and 5(f), and, give the radii mean error of 5.2 % and 4.1 %. Fig. 5(f) also illustrates that the conventional approach has 'over-corrected' the original image shown in Fig. 5(d) and introduces pin-cushion distortion, instead of barrel distortion.

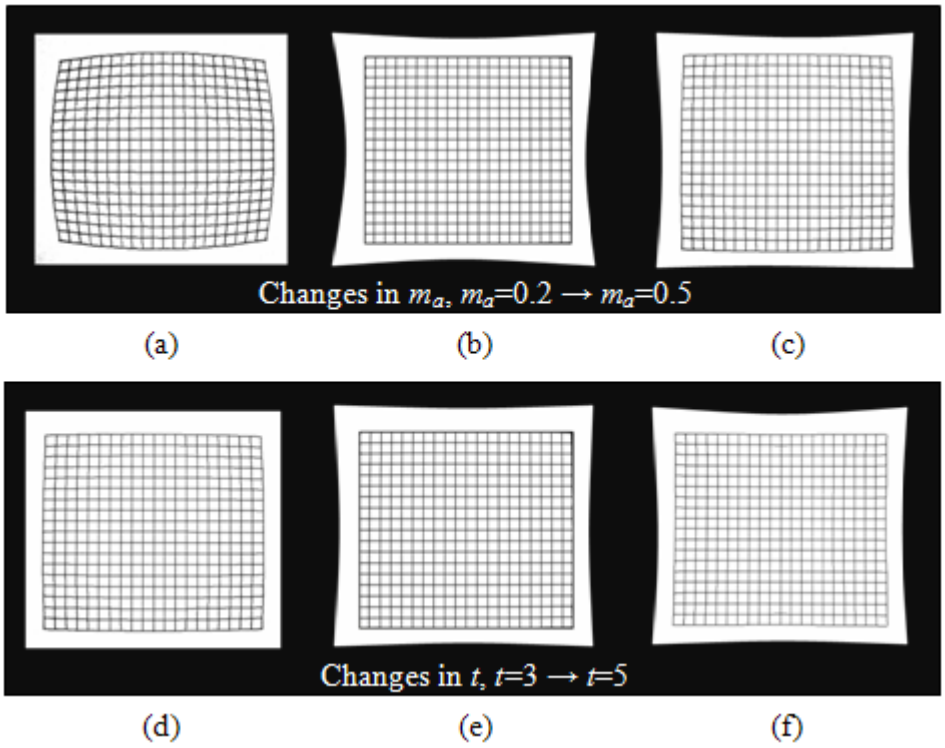

Fig. 5. Corrected Images of Proposed and Conventional Approaches Due to Changes in m_a and t.

The effects of the changes in sensor properties are further evaluated by incrementing the m_a and t values, to investigate the behaviour of the corrected images using the proposed and conventional approaches. Fig. 6 shows the radii mean error of the corrected images using the proposed and conventional approaches, for sensors Case 1 and Case 2 due to incremental changes in sensor properties m_a and t. Fig. 6(a) shows that the corrected images by the proposed approach attains 1.5 % and 1.2 % error for Case 1 and 2 at m_a=0, instead of expected non-existing error. This is because the uncertainties exist in the effective focal length, f_d affect the image coordinates, $\mathbf{x}_u$ and $\mathbf{x}_d$. The proposed approach managed to maintain its corrected image accuracy despite the increasing changes in m_a, achieving the average errors, e_m of 1.5 % and 2.5 % for Case 1 and 2. As illustrated by Fig. 6(b), the approach also able to maintain its corrected image accuracy regardless of increasing changes in another factor t, with average errors e_t of 2.5 % for Case 1 and 3 % for Case 2.

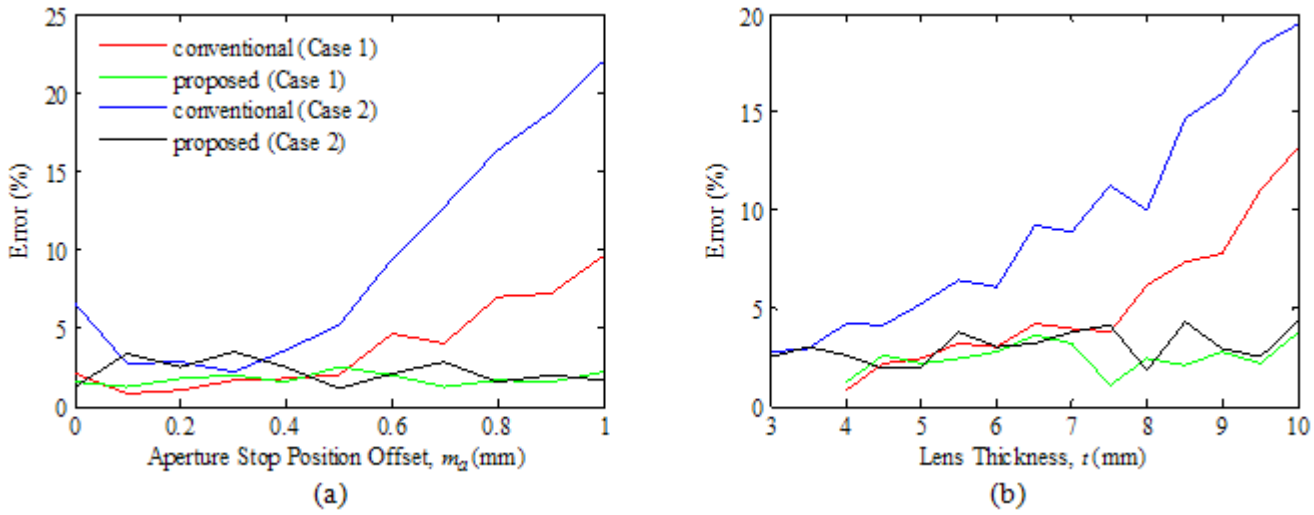

Fig. 6. Numerical Results of Corrected Images Due to Incremental Changes in m_a and t for Case 1 and Case 2.

On the contrary, the corrected images by the conventional approach for Case 1and 2 were unable to maintain its accuracy corresponding to both increasing changes in m_a and t. According to Fig. 6, the radii mean errors for Case 1 increase to the maximum of 9.6 % for changes in m_a and 13.2 % for changes in t. Similarly, the radii mean error for Case 2 has been escalating to the maximum errors of 22.1 % and 19.5 % respectively, as shown in Fig. 6. The maximum errors of the corrected images by the proposed approach are 2.5 % and 3.8 % for Case 1 and 3.5 % and 4.4 % for Case 2 respectively. Fig. 6 also shows that the corrected images by the conventional approach has the lowest percentage error at the specifications given by Table 1, because they are derived based on the image data using these specifications. For both cases, e_t is higher than e_m, and the error of the conventional approach is increasing at a higher rate with changes in t than changes in m_a. These show that t is a more prominent factor than m_a, and as formulated in Section 3, t indirectly affects $\mathbf{x}_d$ and $\mathbf{x}_u$ while m_a affects $\mathbf{x}_d$ only.

The approaches are also evaluated on the basis that the sensor properties, m_a and t are dependent on each other. Fig. 7 shows the numerical results of this evaluation process, where Figs. 7(a) and 7(b) represent results for Case 1 and Figs. 7(c) and 7(d) represent results for Case 2. As illustrated by Figs. 7(a) and 7(c), the actual error escalates at a much higher rate to the maximum error of 22 % for Case 1 and 40 % for Case 2. In contrast to the conventional approach, Figs. 7(b) and 7(d) show the consistency of the corrected images radii mean error using the mechanistic deconvolution approach for both cases, and the average errors are 3.2 % and 4.1 % for Case 1 and 2. Fig. 7 also illustrates that Case 2 has a lower accuracy than Case 1, which supports the fact that better specifications has lower properties uncertainties.

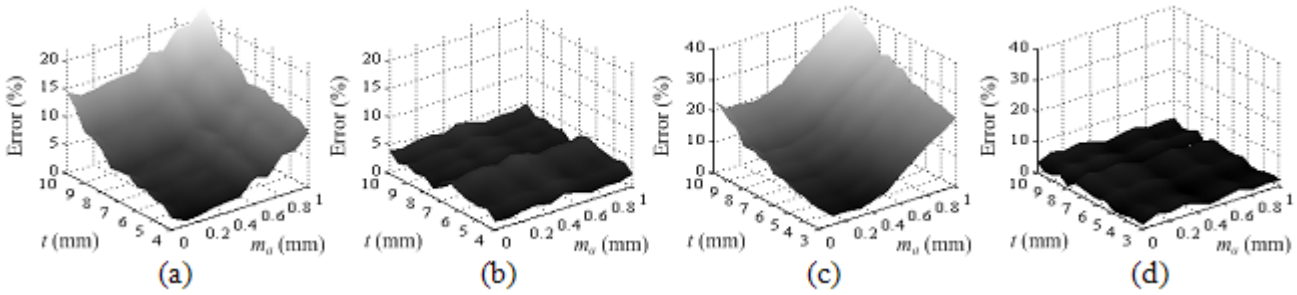

Fig. 7. Numerical Results of Image Correction Due to Dynamic Changes in Sensor Properties.

The mechanistic deconvolution approach was implemented into a simple image recognition system, to determine its efficiency, in comparison to the previously mentioned conventional approach. The image recognition system consists of two modules, which are the colour and pattern recognition. This system was set in a fixed position and was tested by tracking a red round object in the environment. This experiment was conducted in a controlled environment. Table 2 shows the accuracy and time efficiency of the proposed and conventional approaches. The table indicates that the proposed approach provides low percentage error, averaging at 3.3 %, in contrast to the conventional approach percentage error, averaging at 6.7 %. As stated in Table 2, the proposed approach, is able to provide the corrected image in approximately 5 times faster than the conventional approach in each cycle, which results in increasing the speed performance of the image recognition system by 1.5 times as compared with the conventional approach.

Table 2. Comparison between mechanistic deconvolution and conventional approaches in image recognition system.

	% Error		**Time (ms)**			
	Proposed	Conventional	Individual		System	
			Proposed	Conventional	Proposed	Conventional
Cycle 1	3.5	4.3	10	48	110	150
Cycle 2	2.8	8.3	12	45	107	146
Cycle 3	3.3	9.5	11	50	114	149
Cycle 4	3.8	5.1	13	46	111	151
Cycle 5	3.2	6.2	12	52	109	154
Mean	**3.3**	**6.7**	**11.6**	**48.2**	**110.2**	**150**

5. Conclusion

The mechanistic deconvolution approach to modelling an image sensor, without calibration technique, has been presented. The proposed approach has utilized mechanical and electrical properties to determine the effective focal length, and, to estimate the distortion effects inherent in image sensors. This, as a result, has reduced dependency on image data and did not require experimental evaluation of the sensors. Two sensors with different specifications were used to validate the proposed approach, and, the approach managed to provide high accuracy corrected images for the sensors. The proposed approach was then compared with a conventional technique to further evaluate its efficiency. In the efficiency evaluation process, the corrected images derived by the proposed approach achieved accuracy similar to the conventional approach corrected images while considerably reducing the number of iterations.

Robustness of the proposed approach due to changes in image sensor properties was also investigated with the conventional technique, and, using two image sensor properties that are the aperture position offset and lens thickness. The model derived by the proposed approach was not affected by the changes of sensor properties, in contrast to the conventional technique. This model, in addition, showed high and consistent accuracy despite incrementing changes of the sensor properties. Thus, it does not require recalibration if sensor parts are modified. The approach was also implemented into a simple image recognition system and proved to be more efficient, in comparison to the conventional technique. In conclusion, the model is not dependent on image data, while successfully correcting for distortion.

The assumptions made in the proposed approach, however, have limited the applicability and robustness of the method to dynamic environments. This approach can be extended to include tangential distortion, further improving the accuracy of corrected data.

Appendix

This section shows brief formulation of the radii mean error. Given the grid pattern of m by n boxes, and, using position indices i=1, 2, n-1, n and j=1, 2, m-1, m, the radii distance for both corrected images d_{ij}' and ideal grid pattern image d_{ij} are

$$d_{ij}' = \sqrt{\left(u_{ij}' - u_0\right)^2 + \left(v_{ij}' - v_0\right)^2} \tag{35}$$

and

$$d_{ij} = \sqrt{\left(u_{ij} - u_0\right)^2 + \left(v_{ij} - v_0\right)^2} \tag{36}$$

The $[u_{ij}, v_{ij}]$ and $[u_{ij}', v_{ij}']$ are the position coordinates of the ideal grid pattern image and corrected images, and, $[u_0, v_0]$ is the centre position of all images. Using Einstein summation convention, the radii mean error e is

$$\%\text{Error, } e = \frac{1}{mn}\left|\frac{d_{ij} - d_{ij}'}{d_{ij}}\right| \text{r } 100\% \tag{37}$$

References

[1]. F. Remondino and C. Fraser, Digital camera calibrations: Considerations and comparisons, *International Archives of Photogrammetry, Remote Sensing and Spatial Information Sciences*, 36, 5, 2006*, pp.* 266-272.

[2]. G. N. DeSouza and A. C. Kak, Vision for mobile robot navigation: A Survey, *IEEE Transactions on Pattern Analysis and Machine Intelligence,* 24, 2, 2002, pp. 237-267.

[3]. R. Y. Tsai, A versatile camera calibration technique for high-Accuracy 3D machine vision metrology using off-the-Shelf TV cameras and lenses, *IEEE Journal of Robotics and Automation,* 1987, pp. 323-344.

[4]. D. C. Brown, Close-range camera calibration, *Photogrammetric Engineering,* 37, 8, 1971, pp. 855-866.

[5]. J. Weng, P. Cohen and M. Herniou, Camera calibration with distortion models and accuracy evaluation, *IEEE Transactions on Pattern Analysis and Machine Intelligence,* 14, 10, 1992, pp. 965-980.

[6]. S. Graf and T. Hanning, Analytical solving radial distortion parameters, In *Proceedings of the 2005 IEEE Computer Society International Conference on Computer Vision and Pattern Recognition (CVPR' 2005)*, San Diego, CA, USA, 20-25 August 2005, pp. 1104-1109.

[7]. J. Mallon and P. F. Whelan, Precise radial un-distortion of images, In *Proceedings of the 17th International Conference on Pattern Recognition (ICPR' 2004),* Cambridge, England, UK, 23-26 August 2004, pp. 18-21.
[8]. D. G. Bailey, A new approach to lens distortion correction, In *Proceedings Image and Vision Computing New Zealand (IVCNZ' 2002 0,* Auckland, New Zealand, 26-28 November 2002, pp. 59-64.
[9]. S. Park and K. Hong, Practical ways to calculate camera lens distortion for real-time camera calibration, *Pattern Recognition,* 34, 6, 2004, pp. 1199-1206.
[10]. S. J. Maybank and O. D. Faugeras, A theory of self-calibration of a moving camera, *International Journal of Computer Vision,* 8, 2, 1992, pp. 123-151.
[11]. E. E. Hemayed, A survey of camera self-calibration, In *Proceedings of the IEEE Conference on Advanced Video and Signal Based Surveillance (AVSS'2003)*, Miami, Florida, USA, 21-22 July 2003, pp. 352-357.
[12]. Z. Zhang, A flexible new technique for camera calibration, *IEEE Transactions on Pattern Analysis and Machine Intelligence,* 22, 11, 2000, pp. 1330-1334.
[13]. J. Morgan, *Introduction to Geometrical and Physical Optics,* R. E. Krieger Pub. Co., 1953.
[14]. S. H. Lim and T. Furukawa, Optical Sensor Modelling Using Mechanistic Deconvolution, In *The 2nd International Conference on Sensing Technology (ICST' 2007),* Palmerston North, New Zealand, 26-28 November 2007, pp. 387-392.

Guide for Contributors

Aims and Scope

Sensors & Transducers Journal (ISSN 1726-5479) provides an advanced forum for the science and technology of physical, chemical sensors and biosensors. It publishes state-of-the-art reviews, regular research and application specific papers, short notes, letters to Editor and sensors related books reviews as well as academic, practical and commercial information of interest to its readership. Because it is an open access, peer review international journal, papers rapidly published in *Sensors & Transducers Journal* will receive a very high publicity. The journal is published monthly as twelve issues per annual by International Frequency Association (IFSA). In additional, some special sponsored and conference issues published annually.

Topics Covered

Contributions are invited on all aspects of research, development and application of the science and technology of sensors, transducers and sensor instrumentations. Topics include, but are not restricted to:

- Physical, chemical and biosensors;
- Digital, frequency, period, duty-cycle, time interval, PWM, pulse number output sensors and transducers;
- Theory, principles, effects, design, standardization and modeling;
- Smart sensors and systems;
- Sensor instrumentation;
- Virtual instruments;
- Sensors interfaces, buses and networks;
- Signal processing;
- Frequency (period, duty-cycle)-to-digital converters, ADC;
- Technologies and materials;
- Nanosensors;
- Microsystems;
- Applications.

Submission of papers

Articles should be written in English. Authors are invited to submit by e-mail editor@sensorsportal.com 6-14 pages article (including abstract, illustrations (color or grayscale), photos and references) in both: MS Word (doc) and Acrobat (pdf) formats. Detailed preparation instructions, paper example and template of manuscript are available from the journal's webpage: http://www.sensorsportal.com/HTML/DIGEST/Submition.htm Authors must follow the instructions strictly when submitting their manuscripts.

Advertising Information

Advertising orders and enquires may be sent to sales@sensorsportal.com Please download also our media kit: http://www.sensorsportal.com/DOWNLOADS/Media_Kit_2008.pdf